Article:
Singh, H., Sreedharan, S., Tiwari, K. et al. (2019) Two photon excitable graphene quantum dots for structured illumination microscopy and imaging application: lysosome specificity and tissue-dependent imaging. Chemical Communications, 55 (4). pp. 521-524. ISSN: 1359-7345

https://doi.org/10.1039/C8CC08610A

ChemComm

Accepted Manuscript

This article can be cited before page numbers have been issued, to do this please use: H. Singh, S. Sreedharan, K. Tiwari, N. Green, C. Smythe, S. K. Pramanik, J. A. Thomas and A. Das, *Chem. Commun.*, 2018, DOI: 10.1039/C8CC08610A.

ROYAL SOCIETY OF CHEMISTRY

rsc.li/chemcomm

View Article Online
DOI: 10.1039/C8CC08610A

Journal Name

COMMUNICATION

Two photon excitable graphene quantum dots for structured illumination microscopy and imaging application: lysosome specificity and tissue-dependent imaging

Received 00th January 20xx,
Accepted 00th January 20xx

DOI: 10.1039/x0xx00000x

www.rsc.org/

Harwinder Singh,[a $] Sreejesh Sreedharan,[b $] Karishma Tiwari,[a] Nicola H. Green,[cd] Carl Smythe,[e] Sumit Kumar Pramanik,*[a] Jim. A. Thomas*[b] and Amitava Das*[a]

Two-photon active Graphene Quantum Dots (GQDs) are obtained from extracts of the neem root. These biocompatible GQDs are found to be suitable for structured illumination microscopy. Two photon microscopy ensured lysosome specificity of GQDs in live cells and confocal luminescence microscopic studies showed tissue-dependent localization of GQDs in Zebra fish.

Lysosomes are single membrane-bound cytoplasmic organelles and are present in almost all eukaryotic cells. Lysosomes are the major degradative compartment of the endosomal system and the terminal path in the endocytic pathway.[1] Lysosomes also facilitate other fundamental processes such as signaling, plasma membrane repair, and intracellular trafficking.[2, 3] Their function is regulated at transcriptional and post-transcriptional levels and responds to both extracellular and intracellular cues.[3, 4] Lysosomal dysfunction is linked to neurodegenerative disorders such as Parkinson's, Alzheimer's, Huntington's disease and pathogenesis of a plethora of disease conditions including dysfunction of lipid and glucose metabolism, infectious diseases and several immune system disorders.[3, 5] Thus, it is essential to understand and monitor basic biological processes involving lysosomes, ranging from cellular clearance to the control of cellular energy metabolism. However, this intrinsic complexity makes an investigation of endo-lysosomal activity a significant challenge.[6] Therefore, the development of new probes and appropriate methodologies for visualizing the dynamics of lysosomes would be a significant advancement in understanding their functionality and provide insights into lysosome-related diseases. [7]

As conventional fluorescence microscopy is diffraction-limited, it provides insufficient resolution to distinguish between lysosomes and mitochondria.[8] Electron microscopy can definitively differentiate these organelles, but it is incapable of capturing dynamic processes in live cells.[9] To overcome the problem imposed by the optical diffraction limit (of ~220 nm), which limits the spatial and temporal resolution of subcellular features, such as the mammalian cellular lysosome (size ~ 1 µm), structured illumination microscopy (SIM) has recently been developed.[10, 11] Luminophores that are appropriate for SIM studies should have high luminescence intensity and stability towards photo-bleaching.[12] However, many small molecular probes photo-bleach or photo-degrade on continuous irradiation during SIM studies. This limits the use of SIM for real-time, live cell tracking and visualization of lysosomes. Consequently, a photo-stable luminescent probe with high emission intensity would facilitate live cell imaging, potentially at the single-molecule level, and provide a method to unveil detailed features of subcellular organelles as well as crucial dynamic process that are associated with biochemical transformations.[12, 13] Additionally, molecular probes with different luminescent colors would also offer simultaneous multicolor super-resolution imaging and labelling of different subcellular organelles.
In this context, luminescent quantum dots have many attractive properties: in particular, photoluminescence with high quantum yields, and high stability towards photobleaching.[14, 15] These properties have made such materials an attractive choice for imaging studies. The biocompatibility of such materials is also crucial for real-time live cell/ in-vivo imaging and probing endogenous or subcellular biochemical transformations[16-18] and recent studies have revealed that GQDs meet all these criteria. [13, 19, 20] Furthermore, photophysical studies reveal that GQDs are non-blinking and have a large two-photon cross-section. Thus, GQDs can be photo-excited using near-infrared (NIR) irradiation. This helps in avoiding irradiation with deleterious high-energy light, and helps to suppress interference from endogenous background fluorescence as well as providing high penetration into biological materials. [21] These factors, along with their low scattering rates, mean that GQDs provide high signal-to-noise imaging ratios.[21] Such materials are expected to be an attractive candidate for intracellular as well as tissue and *in-vivo*

[a] *CSIR-Central Salt and Marine Chemicals Research Institute, Bhavnagar, Gujarat, India. Email: sumitpramanik007@gmail.com; a.das@csmcri.res.in*
[b] *Department of Chemistry, University of Sheffield, Western Bank, Sheffield, S3 7HF, UK. Email: James.thomas@sheffield.ac.uk*
[c] *Department of Materials Science and Engineering, Kroto Research Institute, North Campus, Broad Lane, University of Sheffield, Sheffield, S3 7HQ, UK*
[d] *INSIGNEO Institute for in silico Medicine, Sheffield, S1 3JD, UK*
[e] *Department of Biomedical Science, University of Sheffield, Sheffield, S3 7HF.*
Electronic Supplementary Information (ESI) available: [details synthetic method of GQDs and experimental methods of biological experiments]. See DOI: 10.1039/x0xx00000x
[$] equally contributing to the work.

imaging.[22, 23] Despite these advantages, reports on biocompatible and two-photon excitable CDs-based probes for specific lysosomal imaging are exceptionally scarce. [24, 25]

Plant materials are generally high in carbon content and are believed to be an excellent source for biocompatible carbon nanomaterials.[26] Neem (*Azadirachta indica*) belongs to Meliaceae family and extracts of variour parts of Neem plant are the rich source of antioxidant. Such extracts are chemo-preventive and show antitumor effects. [27]

In this study, two-photon excitable GQDs are synthesized from extracts of neem plant roots produced by a hydrothermal process. The as-synthesized GQDs exhibit tuneable full-colour emission and are found to be biologically benign. *In-vitro* imaging studies reveal specific localization of these GQDs in lysosomes of live RAW cells. Subsequent *in-vivo* imaging studies performed with live Zebrafish embryos and larvae reveal that the probes display tissue dependent localization. Importantly, these GQDs are found to be suitable for use in SIM as well as two-photon imaging.

Typically, GQDs were prepared following a facile solvothermal approach using Neem plant root extract (ESI†). Upon hydrothermal treatment, graphene oxide sheets were first formed, which subsequently broke down into mono-dispersed GQDs. The as-synthesized GQDs dispersion remained stable, clear and homogeneous at room temperature over months.

Fig. 1a shows the transmission electron microscopy (TEM) images of as-prepared monodisperse GQDs with uniform diameters of 2-5 nm. The high-resolution (HR-TEM) images show that most GQDs have well-resolved lattice structures with a d-spacing value of 0.21 nm (Fig. 1c), in agreement with the basal spacing of graphite. Furthermore, the hydrodynamic diameter of the GQDs, confirmed by DLS, was found to be 8 - 17 nm. The powder X-ray diffraction (pXRD) patterns of the GQDs were measured to identify its crystalline nature (Fig. 1f); the broad diffraction peaks at 2θ = 24.5 with d spacing of 0.30 nm was assigned to the graphite lattice spacing of (002). This confirms that the as-synthesized GQDs are crystalline like graphite (JCPDS No. 75-1621).[28]

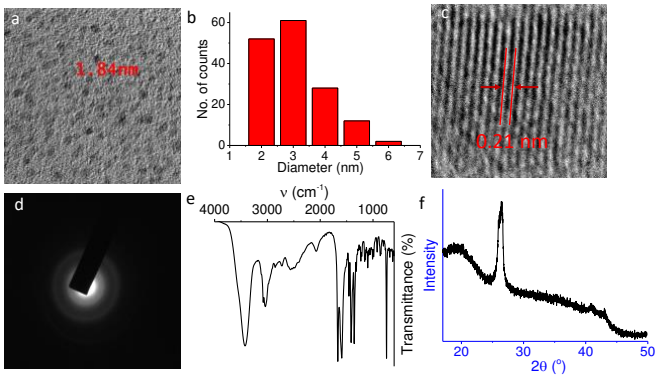

Fig. 1 (a) TEM image of GQDs, (b) diameter distribution of GQDs, (c) HRTEM image of GQD, (d) FFT or SAED pattern of the GQDs, (e) FT-IR spectra of GQDs, (f) powder XRD data of GQDs.

X-ray photoelectron spectroscopy (XPS) and Fourier transform infrared (FT-IR) analysis were carried out to determine the surface functionalities of GQDs. Fig. 2a shows the full XPS spectrum of GQDs with three peaks at 285, 396 and 535 eV, which are ascribed to C1s, N1s and O1s, respectively. [29] These data confirm that the neem root-GQDs are mainly composed of the elements C, N and O. Binding energy values of these GQDs were obtained from the high-resolution spectrum of C1s (Fig. 2b), which showed that carbon has three different chemical environments, corresponding to C=C at 284.3 eV, C–C/C–H at 285.4 eV, and C-O at 287.8 eV. [29] The high-resolution spectrum of O1s (Fig. 2c), showed that C-O-C functionalities are significantly more common than the C=O functionality. Further information on the functional groups on the surface of the GQDs was also obtained from the FT-IR spectra (Fig. 1e). Weak peaks at 2724 and 2858 cm^{-1} were ascribed to the stretching vibrations of –CH.[30] A peak at 1609 cm^{-1} confirmed the aromatic stretching vibration of graphite domains, and a peak at 1340 cm^{-1} was assigned to the stretching vibration of C–O–C.[30]

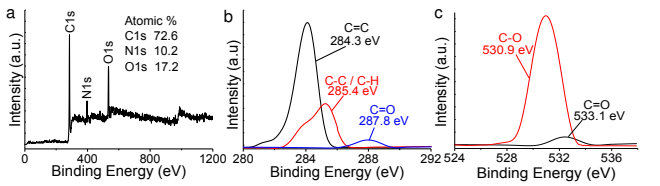

Fig. 2 (a) Full range XPS analysis of GQDs (b & C) high resolution XPS spectra of the C1s and O1s region.

Peaks at 1692 and 1420 cm^{-1} are ascribed to the stretching vibration of C=O and bending vibrations of –OH (in–COOH), respectively.[30] A characteristic absorption peak at around 3440 cm^{-1} is assigned to the stretching vibration of –OH (in–COOH),[30] while peaks at 3406 cm^{-1} (broad) and 1603 cm^{-1} are assigned to N–H stretching and N–H bending vibrations of the amino groups, respectively.[12]

A negative zeta potential of -28.6 mV for the GQDs in aqueous solution further supports the presence of a significant number of carboxylic groups on their surface. These hydrophilic carboxylic groups help to disperse the GQDs in aqueous solution. The unsaturated carbon bonds were further examined by Raman spectroscopy, which showed D-band and G-band features at 1375 cm^{-1} and 1596 cm^{-1}, respectively (Fig. S1). The ratio of the relative intensity of the D and G bands (I_D/I_G) is about 0.96, indicating that the green-emitting QCDs are of disordered nature. [31]

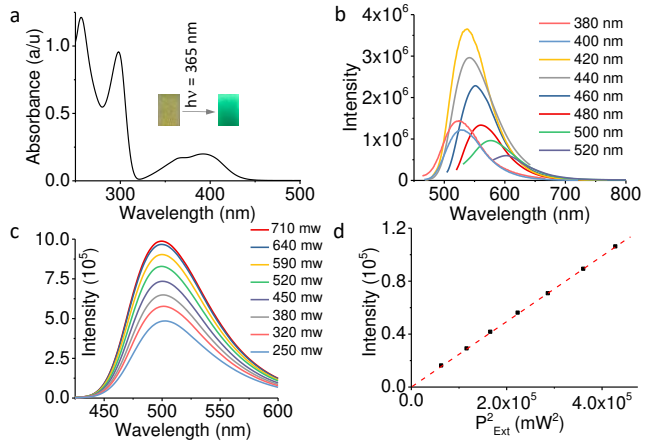

Fig. 3 (a) UV-Vis absorption spectra of the GQDs and in inset images of the green-emitting GQDs under sunlight (left) and UV irradiation (right). (b) Photoluminescence of GQDs aqueous solution under the excitation wavelength of 380-520 nm with 20 nm increments, (c) Two-photon photoluminescence (excitation wavelength = 800 nm) of

aqueous solution of GQDs with different excitation power. (d) Quadratic relationship of the fluorescence intensity of GQDs aqueous solution with the different excitation laser powers at 800 nm (P_{Exc}, as measured at the focal plane).

Absorption band maxima at 288 and 395 nm (Fig. 3a) of the synthesized GQDS were ascribed to the π-π* transition of multiple polyaromatic chromophores and the n-π* transition of carbonyl groups, respectively.[32] Excitation dependent emission spectra, shown in Fig. 3b, are similar to those of previously reported carbon nanoparticles,[32] with a emission maximum at 535 nm observed on excitation at 420 nm. Earlier reports suggest that - owing to aggregation or precipitation processes under physiological conditions - the quantum yield and photostability of GQDs can be relatively low.[33] Strikingly, the newly synthesized GQDs show a strong green luminescence (quantum yield (Φ) of 55%; average of three independent studies), which is comparable to the highest Φ value reported for GQDs.[34] The emission band was found to shift from 535 nm to 605 nm on excitation at 520 nm (Fig. 3b); characteristic of continuous excitation-dependent full-color emission.

The up-conversion (two-photon) luminescence properties of the new GQDs were investigated on a home-built optical setup using a NIR femtosecond pulsed laser (800 nm) as the excitation source. A representative two-photon fluorescence spectrum of GQDs is shown in Fig. S4, which is analogous to the single-photon fluorescence spectrum recorded for the same sample of GQDs: the λ_{Max}^{Ems} is indistinguishable with that of the single-photon fluorescence spectrum of GQDs. To confirm whether the emission of the GQDs on excitation at 900 nm originated from two-photon absorption, the change in green fluorescence intensity as a function of the power of the 900 nm laser was investigated. It was found that the intensity of the fluorescence maximum (λ_{Ext} = 900 nm) is dependent on excitation laser power (Fig. 3c), with the fluorescence intensity displaying a quadratic relationship with laser power (Fig. 3d). All these results are consistent with two-photon excitation processes causing the observed green fluorescence from the GQDs.[35]

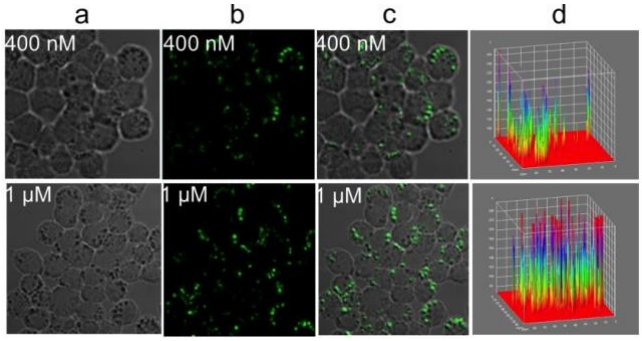

Fig. 4 Optical microscopy images showing uptake of GQDs in live RAW cells: (a) Phase contrast, (b) emission after two-photon absorption, (c) merged image, (d) fluorescence Intensity maps. (Pseudo color has been employed in all the images.) λ_{Ext} = 900 nm.

To examine the suitability of the as-prepared GQDs for cellular imaging, *in-vitro* cellular studies in live RAW cells were performed using up-conversion two-photon microscopy (TPM) and an 900 nm laser as the excitation source. In these condition, bright green luminescence from the cytosol was observed, which also confirmed the cell membrane permeability and cellular internalization of the GQDs (Fig. 4). An increase in the concentration of GQDs incubated with live RAW cells also produced a concomitant increase in intracellular emission (Fig. 4b) and this was confirmed by the 3D intensity profile generated from these data (Fig. 4d). Overlays of the bright-field and luminescent images confirm that the QCDs are primarily localized at the cytoplasmic regions. The punctated nature of the images that was evident in the intensity mapping (Fig. 4d), indicated that the GQDs were localized in specific regions within the cytoplasm. This was investigated in more detail through co-localization studies.

The fluorescence signals in the RAW cells suggested lysosomal localization, as cellular entry by endocytosis would lead to translocation from the extracellular environments into intracellular lysosomes.[36] To confirm specific lysosomal imaging with GQDs, co-localization experiments with the commercial lysosome probe LysoTracker® Deep Red (LTDR) were performed. The spectral properties of LTDR are complementary to those of the GQDs. GQDs were single-photon excited at 488 nm and their emission was collected at 500 to 550 nm, whereas LTDR showed emission at 655 nm following excitation at 644 nm (Fig. 5 and Fig. S5 for RAW and MCF 7 cell line respectively). The high Pearson's coefficient (94%) data confirmed the specific localization of GQDs within the lysosomes of RAW cells (Fig. 5c). Although analogous co-localization experiments, with Mito Tracker Deep Red (MTDR) and Hoechst 33258, were performed (Fig. S6), these studies only confirmed that GQDs were not localized in mitochondria or nuclei. Presumably, the presence of the –COOH, C-O-C and the amino functionalities on the surface 0f the particles help to achieve the appropriate lipophilicity for specific lysosomal localization.[37]

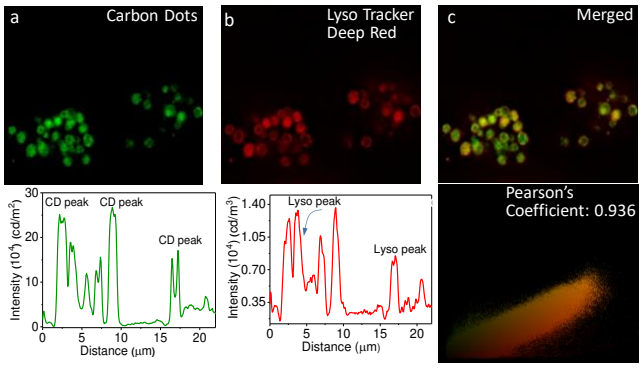

Fig. 5 Colocalization experiments of intracellular localization of GQDs using Lyso Tracker probes in RAW cells: Wide-field microscopy images of in cellular emission of GQDs (panel a) with intensity along the traced line shown underneath. Emission from Lyso Tracker Deep Red (panel b) and intensity along the same line shown below. Panel C shows the overlap of green and red fluorescence, indicating lysosomal localization of GQDs. Panel d shows the Pearson coefficient = 0.936.

After ensuring imaging in a cellular model, experiments with a vertebrate model were performed. Zebrafish were chosen as an *in-vivo* imaging model due to their relatively fast growth time and optical transparency. Often, for in-tissue imaging, these animals are essentially fixed with aldehyde and subjected to injection with the luminescent probe. In this study, Zebrafish embryos and larvae were simply soaked in GQDs and then observed by real-time fluorescence microscopy (Fig. 6). Observations on one hour post fertilization (hpf) Zebrafish embryos exposed to 1 mM GQDs solution for 30 min, confirmed that the GQDs easily enter Zebrafish embryos across the

chorion (chorion pore size: 0.17 µm) and the germ ring around the yolk during socking. Zebrafish larvae at 72 hpf showed strong fluorescence in the specific yolk sac region, which confirmed localization of a high proportion of GQDs in the digestive system.

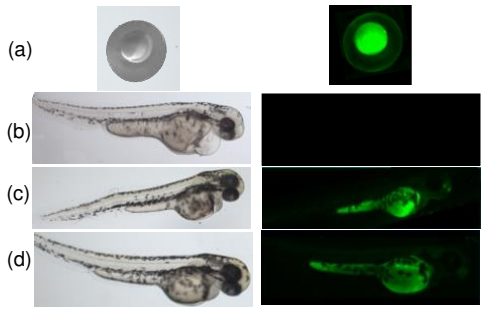

Fig. 6 Bright-field and fluorescence images of zebra fish embryos and larvae after soaking in 1 mg mL^{-1} GQDs solution for 30 min at different time intervals: (a) 1 hpf; (b) 72 hpf; (c) 72 hpf; and (d) 96 hpf. (b) is the control experiment.

The fluorescence emission in other parts of the Zebra Fish larvae at 72 hpf was very weak (Fig. 6c), confirming the tissue-dependent affinity of the GQDs. As there are many similarities between Zebrafish and mammalian lipid metabolisms,[38] GQDs may have potential imaging applications in revealing aspects of lipoprotein and nutritional biology. To study how the larvae retained GQDs, the 72 hpf larvae were first soaked in 1 mM GQDs solution for 1 h. After 1 day, the fluorescent sites in the Zebrafish larvae were found to be identical to those just after soaking (Fig. 6d), this confirms that these GQDs show tissue depended affinity; therefore they may have potential applications in digestive system imaging.

Biocompatibility studies using an MTT assay on the as-synthesized GQDs showed that viability levels in treated cells remained similar to a control group. Indeed, no decrease below 99% was observed, even after exposures to concentrations up to 100 µg/mL of as-synthesized GQDs of up to 24 h (ESI, Fig. S7). This confirms that the GQDs are biocompatible, making them excellent candidates for biomedical applications.

In summary, GQDs were synthesized by a simple and facile hydrothermal method using neem root extract as starting material. The as-synthesized GQDs exhibited excellent biocompatibility, photo-stability, up-conversion and continuous full-color emission. *In-vitro* experiments revealed that the GQDs display specific affinity towards lysosomes, whilst *in-vivo* imaging involving Zebra fish confirmed that GQDs preferentially localize into yolk sac region. These studies indicate that these GQDs can be used as fluorescence imaging agents for the digestive system. This work indicates that - if therapeutic functions are added to the GQDs - they could be used as platforms for constructing intelligent nanomedicines, which integrate diagnostic, targeting, and therapeutic functions.

AD acknowledges SERB grants (EMR/2016/001850 & JCB/2017/000004) and DBT (India) grant BT/PR22251/NNT/ 28/1274/2017) for financial support.

Conflicts of interest

There are no conflicts to declare.

Notes and references

1. H. Savolainen, *Journal of Biological Chemistry*, 2009, **284**, le10.
2. S. Wennekamp, S. Mesecke, F. Nédélec and T. Hiiragi, *Nature Reviews Molecular Cell Biology*, 2013, **14**, 452.
3. C. Settembre, C. Di Malta, V. A. Polito, M. G. Arencibia, F. Vetrini, S. Erdin, S. U. Erdin, T. Huynh, D. Medina, P. Colella, M. Sardiello, D. C. Rubinsztein and A. Ballabio, *Science*, 2011, **332**, 1429-1433.
4. M. Sardiello, M. Palmieri, A. di Ronza, D. L. Medina, M. Valenza, V. A. Gennarino, C. Di Malta, F. Donaudy, V. Embrione, R. S. Polishchuk, S. Banfi, G. Parenti, E. Cattaneo and A. Ballabio, *Science*, 2009, **325**, 473-477.
5. S. Tamar, B. C. Lo, R. Alessandra, W. Christoph, R. R. Annick and F. A. H., *Movement Disorders*, 2011, **26**, 1593-1604.
6. L. Yu, C. K. McPhee, L. Zheng, G. A. Mardones, Y. Rong, J. Peng, N. Mi, Y. Zhao, Z. Liu, F. Wan, D. W. Hailey, V. Oorschot, J. Klumperman, E. H. Baehrecke and M. J. Lenardo, *Nature*, 2010, **465**, 942.
7. D.-Y. Zhang, Y. Zheng, C.-P. Tan, J.-H. Sun, W. Zhang, L.-N. Ji and Z.-W. Mao, *ACS Applied Materials & Interfaces*, 2017, **9**, 6761-6771.
8. Y. Han, M. Li, F. Qiu, M. Zhang and Y.-H. Zhang, *Nature Communications*, 2017, **8**, 1307.
9. N. Liv, D. S. B. van Oosten Slingeland, J.-P. Baudoin, P. Kruit, D. W. Piston and J. P. Hoogenboom, *ACS nano*, 2016, **10**, 265-273.
10. Y. Han, M. Li, F. Qiu, M. Zhang and Y.-H. Zhang, *Nature Communications*, 2017, **8**, 1307.
11. S. Erdinc, *Journal of Physics: Condensed Matter*, 2017, **29**, 273001.
12. S. K. Pramanik, S. Sreedharan, H. Singh, N. H. Green, C. Smythe, J. A. Thomas and A. Das, *Chemical Communications*, 2017, **53**, 12672-12675.
13. L. Wang, B. Wu, W. Li, S. Wang, Z. Li, M. Li, D. Pan and M. Wu, *Advanced Biosystems*, 2018, **2**, 1700191.
14. L. Wang, Y. Wang, T. Xu, H. Liao, C. Yao, Y. Liu, Z. Li, Z. Chen, D. Pan, L. Sun and M. Wu, *Nature Communications*, 2014, **5**, 5357.
15. L. Wang, W. Li, B. Wu, Z. Li, S. Wang, Y. Liu, D. Pan and M. Wu, *Chemical Engineering Journal*, 2016, **300**, 75-82.
16. M. Bottrill and M. Green, *Chemical Communications*, 2011, **47**, 7039-7050.
17. P. Zrazhevskiy, M. Sena and X. Gao, *Chemical Society reviews*, 2010, **39**, 4326-4354.
18. B. R. Smith and S. S. Gambhir, *Chemical Reviews*, 2017, **117**, 901-986.
19. L. Wang, W. Li, M. Li, Q. Su, Z. Li, D. Pan and M. Wu, *ACS Sustainable Chemistry & Engineering*, 2018, **6**, 4711-4716.
20. L. Wang, B. Wu, W. Li, Z. Li, J. Zhan, B. Geng, S. Wang, D. Pan and M. Wu, *Journal of Materials Chemistry B*, 2017, **5**, 5355-5361.
21. S. Zhuo, M. Shao and S.-T. Lee, *ACS Nano*, 2012, **6**, 1059-1064.
22. B. Sapkota, A. Benabbas, H.-Y. G. Lin, W. Liang, P. Champion and M. Wanunu, *ACS Applied Materials & Interfaces*, 2017, **9**, 9378-9387.
23. S. Wang, N. Kharche, E. Costa Girão, X. Feng, K. Müllen, V. Meunier, R. Fasel and P. Ruffieux, *Nano Letters*, 2017, **17**, 4277-4283.
24. J. Bartelmess, E. De Luca, A. Signorelli, M. Baldrighi, M. Becce, R. Brescia, V. Nardone, E. Parisini, L. Echegoyen, P. P. Pompa and S. Giordani, *Nanoscale*, 2014, **6**, 13761-13769.
25. G. Lemenager, E. De Luca, Y.-P. Sun and P. P. Pompa, *Nanoscale*, 2014, **6**, 8617-8623.
26. P. Miao, K. Han, Y. Tang, B. Wang, T. Lin and W. Cheng, *Nanoscale*, 2015, **7**, 1586-1595.
27. F. Hao, S. Kumar, N. Yadav and D. Chandra, *Biochimica et Biophysica Acta (BBA) - Reviews on Cancer*, 2014, **1846**, 247-257.
28. Y. Sun, S. Wang, C. Li, P. Luo, L. Tao, Y. Wei and G. Shi, *Physical Chemistry Chemical Physics*, 2013, **15**, 9907-9913.
29. Y. Tian, L. Li, X. Guo, A. Wójtowicz, L. Estevez, M. J. Krysmann and A. Kelarakis, *Chemical Communications*, 2018, **54**, 9067-9070.
30. T. Gao, X. Wang, L.-Y. Yang, H. He, X.-X. Ba, J. Zhao, F.-L. Jiang and Y. Liu, *ACS Applied Materials & Interfaces*, 2017, **9**, 24846-24856.
31. D. Liu, X. Chen, Y. Hu, T. Sun, Z. Song, Y. Zheng, Y. Cao, Z. Cai, M. Cao, L. Peng, Y. Huang, L. Du, W. Yang, G. Chen, D. Wei, A. T. S. Wee and D. Wei, *Nature Communications*, 2018, **9**, 193.
32. H. Ding, S.-B. Yu, J.-S. Wei and H.-M. Xiong, *ACS Nano*, 2016, **10**, 484-491.
33. R. Guo, S. Zhou, Y. Li, X. Li, L. Fan and N. H. Voelcker, *ACS Applied Materials & Interfaces*, 2015, **7**, 23958-23966.
34. V. B. Kumar, Z. e. Porat and A. Gedanken, *Ultrasonics Sonochemistry*, 2016, **28**, 367-375.
35. L. Cao, X. Wang, M. J. Meziani, F. Lu, H. Wang, P. G. Luo, Y. Lin, B. A. Harruff, L. M. Veca, D. Murray, S.-Y. Xie and Y.-P. Sun, *Journal of the American Chemical Society*, 2007, **129**, 11318-11319.
36. S. Salatin and A. Yari Khosroushahi, *Journal of Cellular and Molecular Medicine*, 2017, **21**, 1668-1686.
37. H. Yu, Y. Xiao and L. Jin, *Journal of the American Chemical Society*, 2012, **134**, 17486-17489.
38. R. L. Miyares, V. B. de Rezende and S. A. Farber, *Disease Models & Mechanisms*, 2014, **7**, 915-927.

View Article Online
DOI: 10.1039/C8CC08610A

Graphical Abstract:

Two photon excitable graphene quantum dots for structured illumination microscopy and imaging application: lysosome specificity and tissue-dependent imaging

Harwinder Singh, Sreejesh Sreedharan, Karishma Tiwari, Nicola H. Green, Carl Smythe, Sumit Kumar Pramanik, Jim. A. Thomas and Amitava Das